Electronic Supplementary Information

Solid-State Activation of Li_2O_2 oxidation Kinetics and Implications for Li-O_2 batteries

Koffi P. C. Yao,[a] Marcel Risch,[b] Sayed Youssef Sayed,[b,†] Yueh-Lin Lee, [b] Jonathon Harding,[c] Alexis Grimaud,[a,‡] Nir Pour,[b] Zhichuan Xu,[d] Jigang Zhou,[e] Azzam Mansour,[f] Fanny Bardé,[g] Yang Shao-Horn*[a,h]

[a] *Department of Mechanical Engineering and the Electrochemical Energy Laboratory, Massachusetts Institute of Technology, 77 Massachusetts Avenue, Cambridge, MA 02139, USA. Email:shaohorn@mit.edu*

[b] *The Research Laboratory of Electronics, Massachusetts Institute of Technology, 77 Massachusetts Avenue, Cambridge, MA 02139, USA*

[c] *Department of Chemical Engineering and the Electrochemical Energy Laboratory, Massachusetts Institute of Technology, 77 Massachusetts Avenue, Cambridge, MA 02139, USA. Email:shaohorn@mit.edu*

[d] *School of Materials Science and Engineering, Nanyang Technological University, 50 Nanyang Avenue, Singapore 639798*

[e] *Canadian Light Source Inc., University of Saskatchewan, Saskatoon, SK S7N 0X4, CANADA*

[f] *Naval Surface Warfare Center, Carderock Division, West Bethesda, Maryland 20817-5700, USA*

[g] *Toyota Motor Europe, Research & Development 3, Advanced Technology 1, Hoge Wei 33 B, B-1930 Zaventem, Belgium*

[h] *Department of Materials Science and Engineering, Massachusetts Institute of Technology, 77 Massachusetts Avenue, Cambridge, MA 02139, USA*

The authors acknowledge the contribution of Nagore Ortiz-Vitoriano in the collection and analysis of XRD data of the Mo-promoted electrode presented in the electronic supplementary information.

Present addresses

‡Author Alexis Grimaud: FRE 3677 "Chimie du Solide et Energie", College de France, 11 Place Marcelin Berthelot, 75231 Paris Cedex 05, France

†Author Sayed Youssef Sayed: Department of Chemistry, Faculty of Science, Cairo University, Giza 12613, Egypt

X-ray diffraction of synthesized α-MnO_2 nanowires

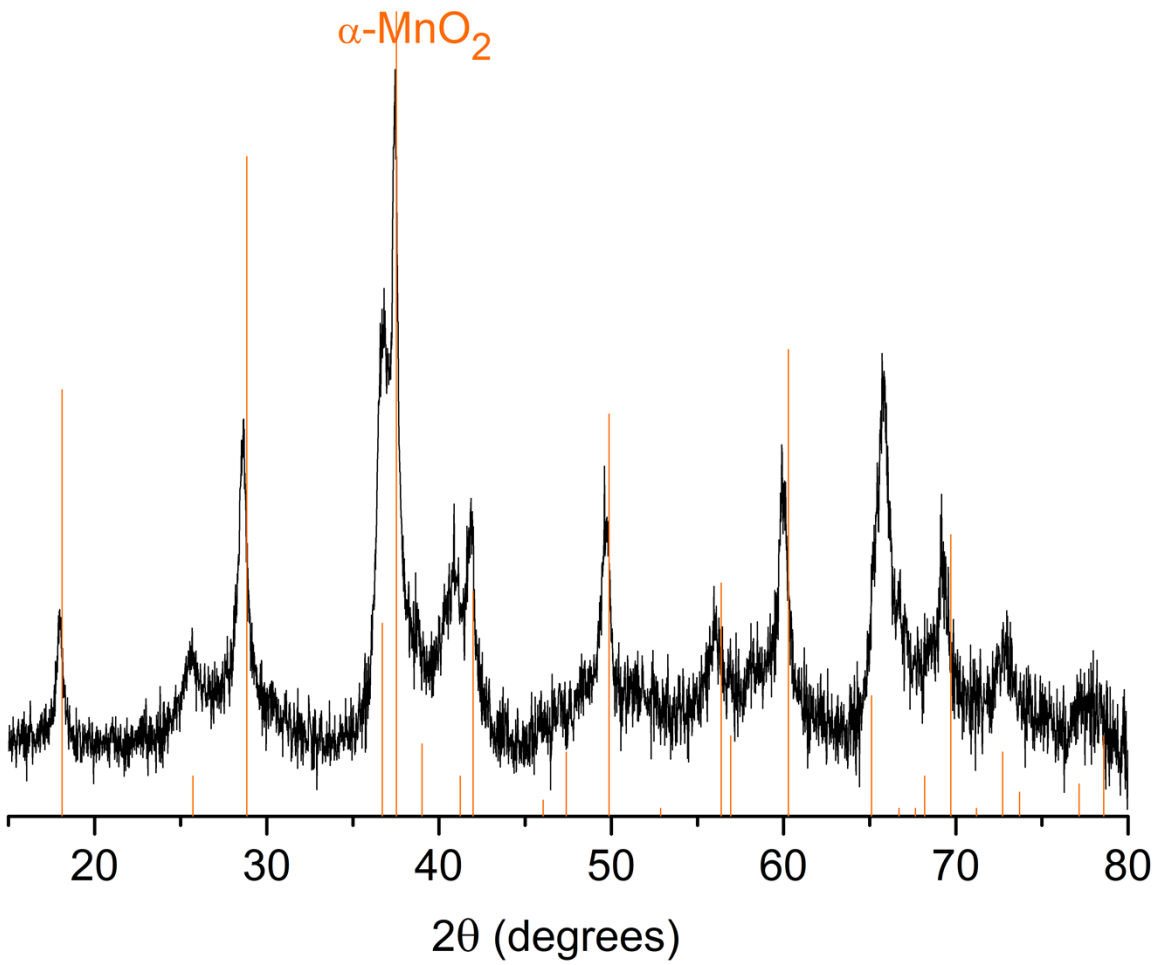

Fig. S1: X-ray diffraction pattern of in-house synthesized α-MnO_2 nanowires. All major peaks of α-MnO_2 are resolved confirming the effective synthesis of the intended phase.

Electrochemical activities of Cr and Mo in carbon-based electrodes

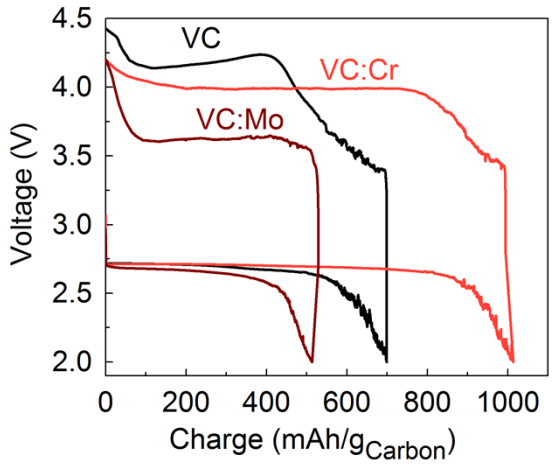

Fig. S2: Galvanostatic performance of carbon-containing VC: promoter::LiNafion = 1:0.667:1 (mass ratios) air electrodes at 100 mA/g_{Carbon}. The increased activity of Cr and Mo promoted is confirmed during charging after discharge (in operando formation of Li_2O_2 followed by its oxidation).

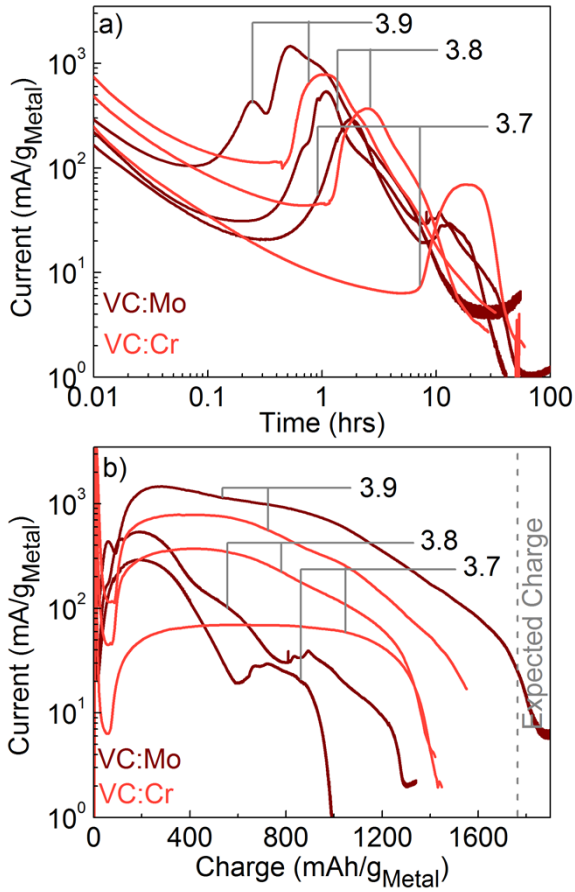

Fig. S3: Potential dependent Li_2O_2 oxidation activity of carbon-containing VC:Cr,Mo:Li_2O_2:LiNafion = 1:0.667:1:1 electrodes compared at 3.7, 3.8, and 3.9 V_{Li}. (a) Current profile vs. time; (b) Current profile vs. charge

X-ray absorption spectroscopy of Cr nanopowder

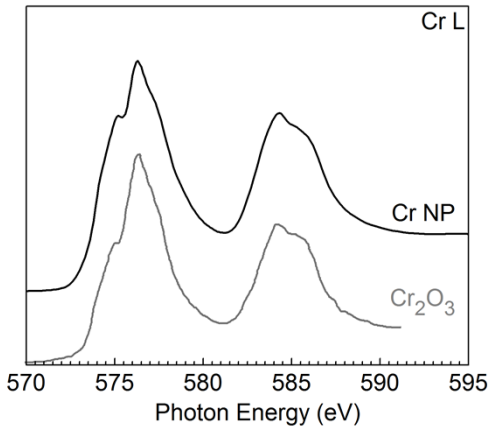

Fig. S4: Cr L edge TEY XAS of Cr nanopowder versus Cr_2O_3.[1] Both edges show that the surfaces of Cr is oxidized to Cr^{3+} in a Cr_2O_3-like environment. This observation is corroborated by XPS as reported previously.[2]

Transition metal L edge spectra of Mo nanopowder showing oxidation state of the nanoparticle surfaces

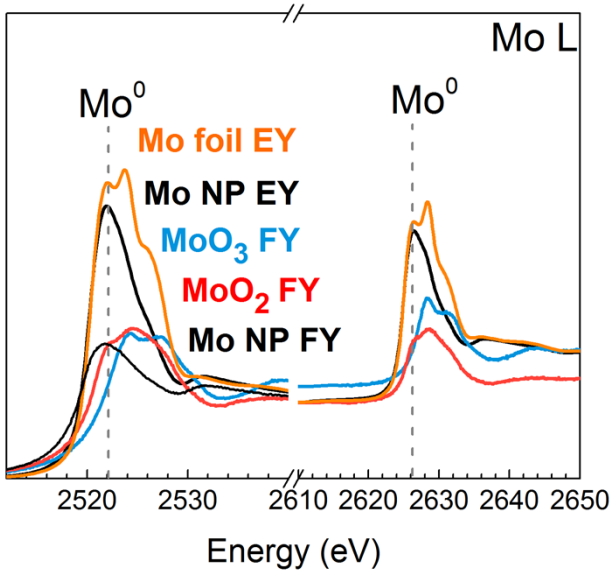

Fig. S5: Mo L edge spectra of Mo nanopowder compared with those collected from reference MoO_3, MoO_2 and Mo foil, which indicate that the oxide layer on Mo powder is relatively thin. This thin Mo layer likely allowed access to the bulk Mo metal for the formation of XRD detectable Li_2MoO_4 as shown below in Fig. S5.

X-ray diffraction pattern of half-charged carbon-free Mo-catalyzed electrode

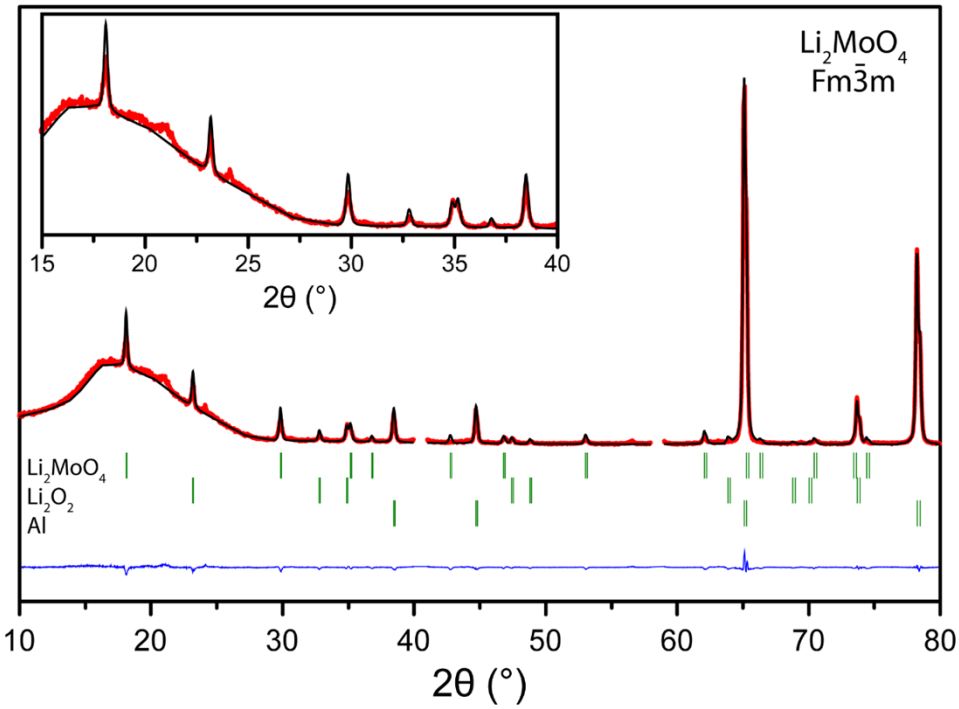

Fig. S6: XRD of pristine Mo:Li_2O_2 (0.667:1) electrode. Clear evidence of Li_2MoO_4 is observed prior to electrochemical treatment which attests of the strong chemical conversion of Mo with Li_2O_2.

Transition metal L edge spectra of Co nanopowder showing oxidation state of the nanoparticle surfaces

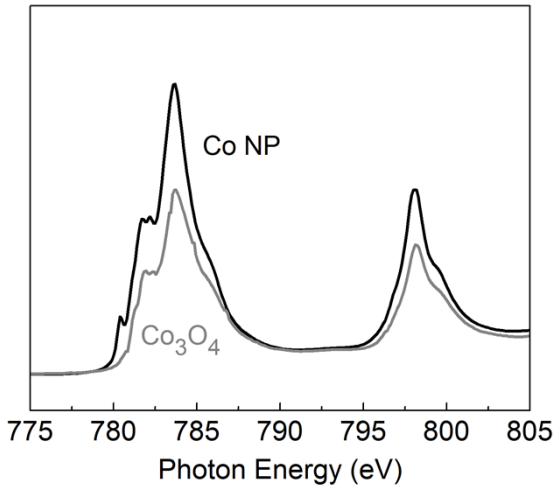

Fig. S7: Co L edge TEY spectra of Co nanoparticles compared to Co_3O_4 shows that the surfaces of Co nanoparticles are mostly oxidized to a Co_3O_4 layer.

Transition metal L edge spectra of Cr catalyzed electrodes at various state of charge

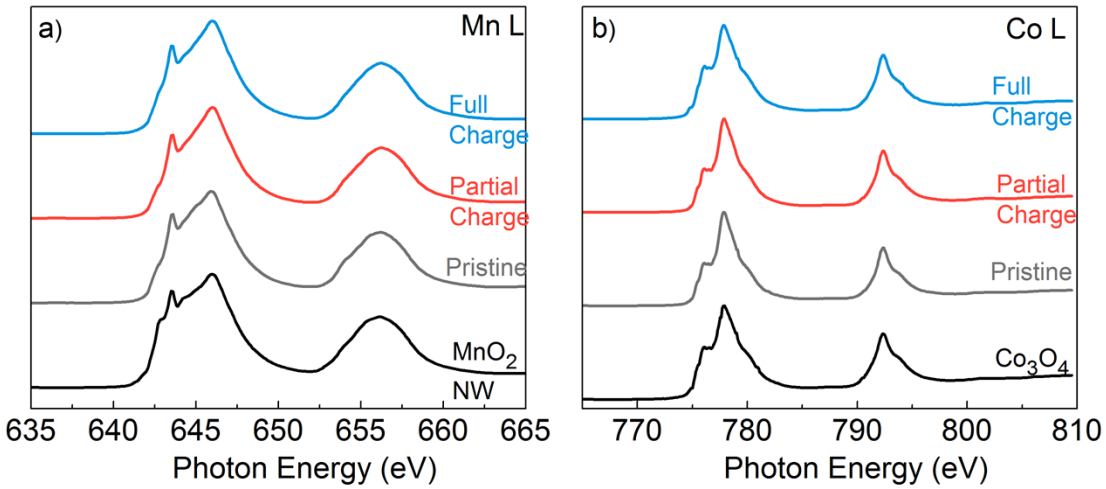

Fig. S8: Metal L edge spectra of oxides MnO_2 and Co_3O_4 nanoparticles, pristine, half-charged, and fully charged carbon-free electrodes in the surface sensitive total electron yield (TEY) mode. Half and full charging for the electrodes examined here was performed at 3.9 V_{Li}.

Verifying the absence of redox mediator effect during enhancement of Li_2O_2 oxidation reaction using transition metal oxides

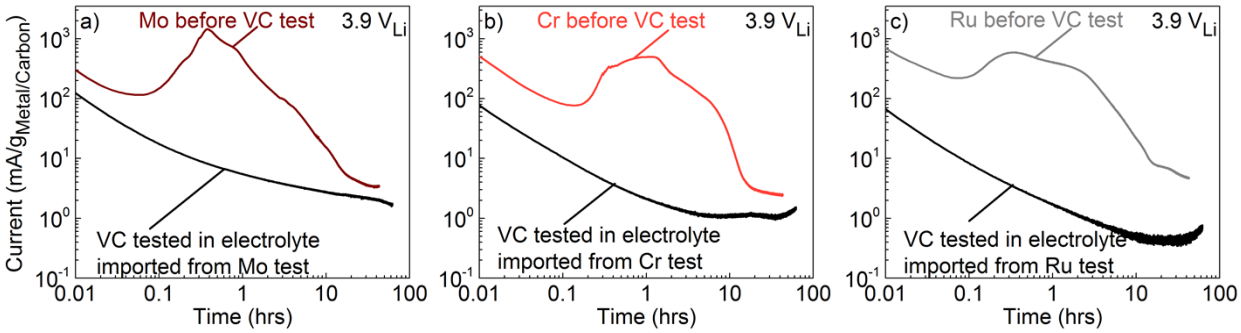

Fig. S9: Effect of impurities (transition metal species dissolved in the electrolyte, water, and other in operando impurities) during Li_2O_2 oxidation in (a) Mo-promoted electrodes, (b) Cr-promoted electrodes, and (c) Ru-promoted electrodes tested by substituting a VC-promoted (VC:Li_2O_2:LiNafion = 1:1:1) electrode into the cell immediately after full charge of a VC: promoter:Li_2O_2:LiNafion = 1:0.667:1:1. ICP-AES data revealed that dissolved metal cations from the preceding promoted electrodes charged at 3.9 V_{Li} were present. The inactivity of the VC-only electrode thus tested suggests that the dissolved cations are not the source of activity in promoted electrodes.

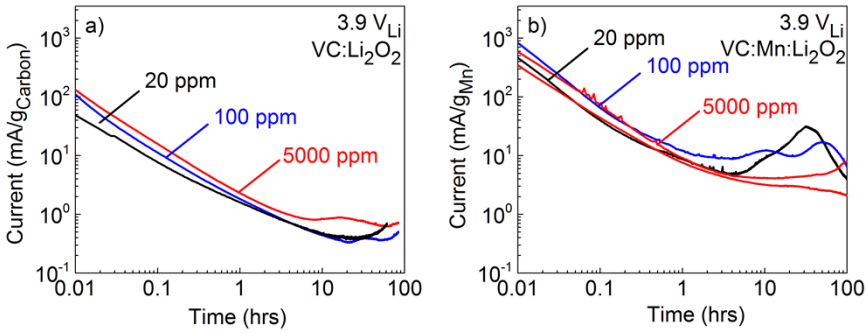

Fig. S10: Effect of electrolyte water (baseline 20 ppm, 100 ppm, and 5000 ppm) content on the activation of Li_2O_2 oxidation in (a) VC-promoted (VC:Li_2O_2:LiNafion = 1:1:1) and (b) the least active Mn-promoted (VC:Mn:Li_2O_2:LiNafion = 1:0.667:1:1). A slightly lowered activation time might be evident in the VC-promoted electrode at the increased water content of 5000 ppm, although still on the order of 10 hours compared to less than 1 hour in high activity Mo, Cr, and Ru promoted electrodes. The overall activity (average current at the applied voltage of 3.9 V_{Li}, <20 $mA/g_{promoter}$) was not significantly enhanced at higher water contents. In the case of Mn-promoted electrodes, addition of water appears detrimental to activity.

Derivation of current rate as function of enthalpies of conversion and applied delithiation overpotential

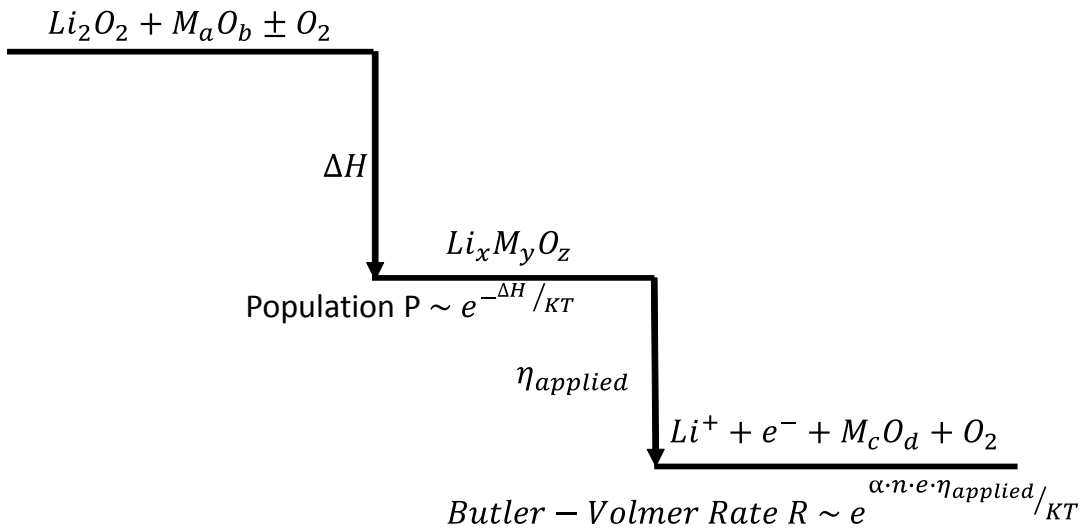

Fig. S11: Schematic of proposed mechanism of chemical conversion of chemical conversion of Li_2O_2 and catalyst to $Li_xM_yO_z$ followed by delithiation.

Derivation of log(i) as a function of enthalpy of conversion and applied overpotential.

The symbol '~' is used to signify 'proportional to'

$$i \sim P \cdot R \sim e^{-\Delta H/KT} \cdot e^{\alpha \cdot n \cdot e \cdot \eta_{applied}/KT}$$

$$\Rightarrow i \sim e^{-\Delta H + \alpha \cdot n \cdot e \cdot \eta_{applied}/KT}$$

$$\log(i) \sim -\Delta H + \alpha \cdot n \cdot e \cdot \eta_{applied}$$

Thermodynamic data of Li_2O_2 reaction with transition metal (oxides) towards formation of lithiated metal oxides.

Table S1: List of potential reactions of the type $Li_2O_2 + M_aO_b \pm O_2 \rightarrow Li_xM_yO_z$ and associated enthalpy of reaction using the materials project database.[3]

Reaction Number	Catalyst	Reaction	Enthalpy of reaction per mole of Catalyst (kJ/mol)
1	MnO_2	$Li_2O_2 + MnO_2 \leftrightharpoons 1/2\ O_2 + Li_2MnO_3$	-104.5
2		$Li_2O_2 + 2/3MnO_2 \rightleftharpoons 1/3O_2 + 2/3Li_3MnO_4$	-56.5
3		$Li_2O_2 + 4MnO_2 \leftrightharpoons O_2 + 2LiMn_2O_4$	-13.5
3	Mn_3O_4	$Li_2O_2 + 1/3Mn_3O_4 \leftrightharpoons 1/6\ O_2 + Li_2MnO_3$	-492
4		$Li_2O_2 + 2/9Mn_3O_4 \rightleftharpoons 1/9O_2 + 2/3Li_3MnO_4$	-349
5		$Li_2O_2 + 4/3Mn_3O_4 + 1/3O_2 \rightleftharpoons 2Li_3MnO_4$	-218
6	Co_3O_4	$Li_2O_2 + 2/3Co_3O_4 \leftrightharpoons 1/3O_2 + 2LiCoO_2$	-151
7	Cr_2O_3	$Li_2O_2 + Cr_2O_3 + O_2 \leftrightharpoons Li_2Cr_2O_7$	-247
8		$Li_2O_2 + 3Cr_2O_3 + 5/2O_2 \leftrightharpoons 2LiCr_3O_8$	-137.17
9		$Li_2O_2 + Cr_2O_3 \leftrightharpoons 1/2O_2 + 2LiCrO_2$	-82
10		$Li_2O_2 + 1/2Cr_2O_3 + 1/2O_2 \leftrightharpoons Li_2CrO_4$	-440
11		$Li_2O_2 + 1/3Cr_2O_3 \leftrightharpoons 1/6O_2 + 2/3Li_3CrO_4$	-338
12		$Li_2O_2 + Cr_2O_3 + O_2 \leftrightharpoons Li_2Cr_2O_7$	-247
13	Mo	$Li_2O_2 + Mo + O_2 \leftrightharpoons Li_2MoO_4$	-939
14		$Li_2O_2 + 1/2Mo + 1/4O_2 \leftrightharpoons 1/2Li_4MoO_5$	-952
15		$Li_2O_2 + 2/3Mo + 1/6O_2 \leftrightharpoons 1/3Li_6Mo_2O_7$	-603.75
16		$Li_2O_2 + Mo + 1/2O_2 \leftrightharpoons Li_2MoO_3$	-645
17		$Li_2O_2 + 2Mo + O_2 \leftrightharpoons 2LiMoO_2$	-473.5
18		$Li_2O_2 + 3/2Mo + O_2 \leftrightharpoons 1/2Li_4Mo_3O_8$	-609
19		$Li_2O_2 + 5/2Mo + 13/4O_2 \leftrightharpoons Li_4Mo_5O_{17}$	-837.3
20	MoO_3	$Li_2O_2 + MoO_3 \leftrightharpoons Li_2MoO_4 + 1/2O_2$	-158
18	Ru	$Li_2O_2 + Ru + 1/2O_2 \leftrightharpoons Li_2RuO_3$	-446
19		$Li_2O_2 + 2/7Ru \leftrightharpoons 1/7O_2 + 2/7Li_7RuO_6$	-463.5
20		$Li_2O_2 + 2Ru + O_2 \leftrightharpoons 2LiRuO_2$	-290.5
21	RuO_2	$Li_2O_2 + RuO_2 \rightleftharpoons 1/2O_2 + Li_2RuO_3$	-19.5
22		$Li_2O_2 + 2/7RuO_2 \rightleftharpoons 3/7O_2 + 2/7Li_7RuO_6$	-37

Theoretical analysis of expected catalytic activity under mechanism of chemical conversion of Li_2O_2 and catalyst to $Li_xM_yO_z$ followed by delithiation

Table S2: Estimated values of $\log(i) \sim -\Delta H + \alpha \cdot n \cdot e \cdot \eta_{applied}$ assuming α ≈ 0.5 and n is the number of Li^+ cations in the lithiated compound.

Catalysts	Intermediate Lithiated compound	$-\Delta H(kJ/r$	E_{rev} (V)	η at 3.9 V_{Li}	$\alpha \cdot n \cdot e \cdot \eta$ (eV)	$(-\Delta H + \alpha \cdot n \cdot e \cdot \eta)$
MnO_2	Li_2MnO_3	-104.5	4.6[4]	-0.7	-0.7	N/A (η < 0)
Mn, Mn_3O_4	Li_2MnO_3	-492	4.6	-0.7	-0.7	N/A (η < 0)
Cr,Cr_2O_3	Li_2CrO_4	-440	3.7[5]	0.2	0.2	4.78
Mo	Li_2MoO_4	-939	2.0[6]	1.9	1.9	11.66
Ru	Li_2RuO_3	-446	3.5[7, 8]	0.4	0.4	5.04
RuO_2	Li_2RuO_3	-37	3.5[7, 8]	0.4	0.4	0.78
Co, Co_3O_4	$LiCoO_2$	-151	3.8[9]	0.1	0.1	1.62

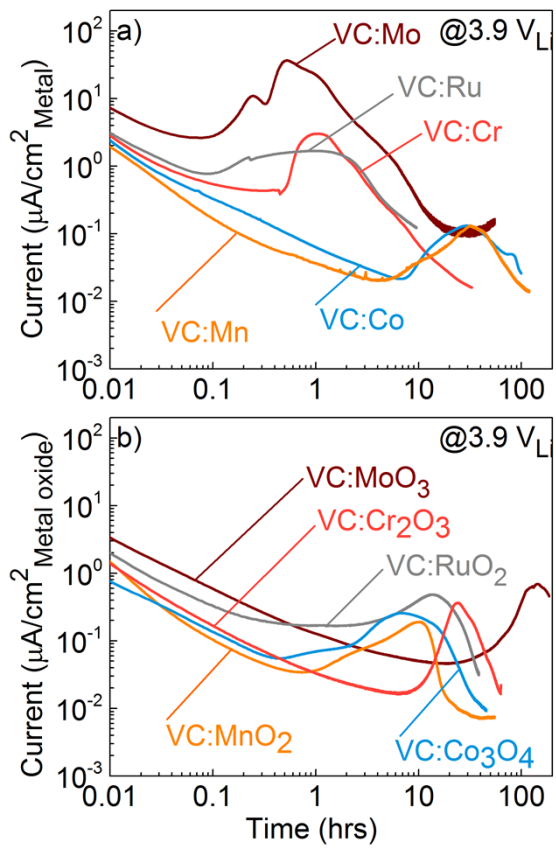

Fig. S12: Electrochemical performance of carbon-containing VC: promoter:Li_2O_2:LiNafion = 1:0.667:1:1 (mass ratios) electrodes at 3.9 V_{Li}. (a) Current per promoter BET surface area *vs.* time for metal nanoparticles promoted electrodes. (b) Current per promoter BET surface area *vs.* time for metal oxide nanoparticles promoted electrodes. Separation of (a) and (b) is for clarity purposes.

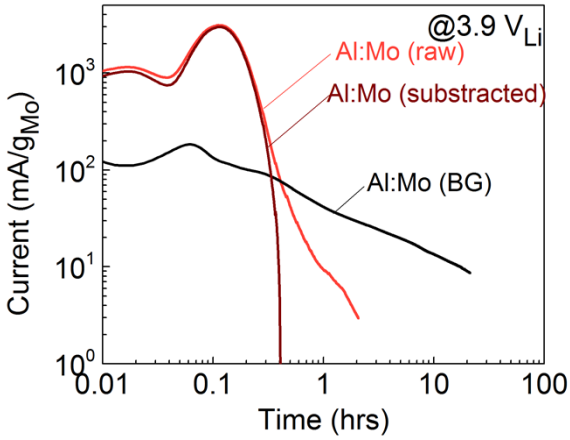

Fig. S13: Electrochemical performance of carbon-free Mo:Li_2O_2 = 0.667:1 (mass ratios, supported on aluminium foil) electrodes at 3.9 V_{Li} and associated background current (Mo on Al foil without Li_2O_2). Upon subtracting the background current from the Li_2O_2 oxidation current, it is clear that the large current observed in Mo-promoted electrodes cannot be attributed electrolyte decomposition by Mo but rather Li_2O_2 oxidation.

References

1 T. Neisius, C. T. Simmons and K. Köhler, *Langmuir*, 1996, **12**, 6377.
2 K. P. C. Yao, Y.-C. Lu, C. V. Amanchukwu, D. G. Kwabi, M. Risch, J. Zhou, A. Grimaud, P. T. Hammond, F. Barde and Y. Shao-Horn, *Phys. Chem. Chem. Phys.*, 2014, **16**, 2297.
3 A. Jain, G. Hautier, S. P. Ong, C. J. Moore, C. C. Fischer, K. A. Persson and G. Ceder, *Phys. Rev. B*, 2011, **84**, 045115.
4 F. Zhou, M. Cococcioni, C. Marianetti, D. Morgan and G. Ceder, *Phys. Rev. B*, 2004, **70**, 235121.
5 L. Zhang and H. Noguchi, *J. Electrochem. Soc.*, 2003, **150**, A601.
6 X. Liu, Y. Lyu, Z. Zhang, H. Li, Y.-s. Hu, Z. Wang, Y. Zhao, Q. Kuang, Y. Dong, Z. Liang, Q. Fan and L. Chen, 2014, **6**, 13660.
7 H. Kobayashi, R. Kanno, Y. Kawamoto, M. Tabuchi, O. Nakamura and M. Takano, *Solid State Ionics*, 1995, **82**, 25.
8 S. Sarkar, P. Mahale and S. Mitra, *J. Electrochem. Soc.*, 2014, **161**, A934.
9 K. Mizushima, P. C. Jones, P. J. Wiseman and J. B. Goodenough, *Solid State Ionics*, 1981, **3–4**, 171.